Supplementary Materials: Catalytic DNA Polymerization Can Be Expedited by Active Product Release

Pepijn G. Moerman[1], Momcilo Gavrilov[2], Taekjip Ha[2,3,4], and Rebecca Schulman[1,5,6,*]

[1] *Chemical and Biomolecular Engineering, Johns Hopkins University, Baltimore, MD 21218, USA*
[2] *Biophysics & Biophysical Chemistry, Johns Hopkins University, Baltimore, MD 21205, USA*
[3] *Biomedical Engineering, Johns Hopkins University, Baltimore, MD 21218, USA*
[4] *Howard Hughes Medical Institute, Baltimore, MD 21205, USA*
[5] *Chemistry, Johns Hopkins University, Baltimore, MD 21218, USA*
[6] *Computer Science, Johns Hopkins University, Baltimore, MD 21218, USA*
[*] *Correspondence should be addressed to: rschulm3@jhu.edu*

1 Supplementary Methods

1.1 Materials

Bst Large Fragment DNA polymerase was purchased from New England Biolabs (NEB). RepX helicase was produced and purified in house as described in the *Helicase Production* section below. All DNA strands were ordered as desalted 100 µM solutions without further purification from Integrated DNA Technologies (IDT), except for strands labeled with the quencher Iowa Black FQ, which were HPLC purified. All strands were used as provided. 10x Thermopol buffer, 1 M $MgSO_4$, 10 mM ATP solution and 100 mM ATP solution were purchased from NEB. TAE (Tris-Acetate-EDTA, 50x) was ordered from Thermo Scientific. 1 mM dNTP solutions were ordered from Promega Corporation. All reporter complexes (see Fig.2b, Fig.4a) were annealed (held at 90 ^{o}C and cooled down to 20 ^{o}C at 1 ^{o}C per minute) at 10 µM with a 1.2x excess of quencher strand. Hairpin strands were used as provided and not annealed or snap cooled. All DNA and enzymes were stored at -20 ^{o}C. Annealed DNA complexes were stored at 4 ^{o}C.

1.2 Helicase production

Escherichia coli Rep helicase is a two-domain enzymze that has two conformations: open and closed. Only the closed conformation is associated with helicase activity. Arslan *et al.* showed that cross-linking the two domains of RepX into the closed conformation enhances its helicase activity and processivity[2]; they named this cross-linked enhanced helicase RepX.

Rep helicase was purified and crosslinked as described previously [2], using a standard Ni-NTA purification column, followed by a single-stranded DNA cellulose column, BMOE (bismaleimidoethane) crosslinking, and dialysis. Briefly, a pET28a(+) vector containing Rep-DM4 was transformed into *E. Coli* BL21(DE3). Cells were grown and induced at OD600 = 0.6 with 0.5 mM IPTG and harvested after an overnight incubation at 18^{o}C. Cell pellets, previously stored at -80^oC, were re-suspended in a sucrose-based lysis buffer and sonicated followed by centrifugation at $34,864\times$g. N-terminally 6xHis-tagged Rep protein was purified using an Ni-NTA column and eluted with 150 mM imidazole-containing buffer, followed by loading the protein into a single-stranded DNA cellulose column, washing, and elution with 1 M NaCl. The presence of the 6xHis should not affect any downstream application. The protein concentration was always kept below 4 mg/ml (50 mM) to avoid aggregation, and the final Rep protein was stored at –20^{o}C or -80^oC with 50% glycerol. Rep crosslinking (RepX) was performed using 10 mM BMOE crosslinker solution in DMF. Optimal crosslinking was achieved at a Rep concentration of 20–25 uM and the final molar ratio of Rep and BMOE was 1 to 5. Excess imidazole and crosslinker were removed by overnight dialysis in 600 mM NaCl. Rep-X was finally stored in 50 μL aliquots at -80^oC in storage buffer (50% glycerol, 600 mM NaCl, 50 mM Tris, pH 7.6).

1.3 Sample preparation

We followed the experimental protocol for the primer exchange reaction outlined by Kishi *et al.*[1]. Unless otherwise indicated, all PER rate measurements were performed in solutions containing 100 µM of each dCTP, dATP, and dTTP, 1x Thermopol buffer, 8 U/ µL Bst Large Fragment DNA polymerase and an additional 12.5 mM $MgSO_4$ to a final concentration of 14.5 mM. No dGTP is added to any experiments so that the need for the polymerase to incorporate a guanine into the nascent strand acts makes a cytosine and effective stop sequence. A typical experiment contains 200 nM of reactant or primer strand, 200 nM of reporter complex and 10 nM of hairpin strand, but we have varied the concentrations and details are provided at the relevant experiments. In

experiments using helicase to speed up PER, the sample contained 100 nM RepX helicase and 1 mM ATP. Otherwise the buffer conditions are the same as in experiments without helicase. Experiments to test RepX function on various reporter complexes contained 10 mM Tris-HCl, 50 mM NaCl, 10 mM $MgCl_2$, and 100 nM reporter complex, with varying amounts of ATP and RepX helicase. All solutions are mixed by vortexing, except those containing Thermopol buffer or enzymes. Instead, those are mixed by pipetting 90 % of the sample volume 3 times up and down within the well.

1.4 Fluorescence measurements

Fluorescence measurements are performed using a Synergy H1 platerader by Biotek, operated using the Gen5 3.08 software. The platereader was loaded with either Corning low volume 384-well polystyrene plates, or conical 96-well plates. The sample volume was 35 µL in the 384-well plates and 50 µL in the 96-well plates. In each experiment all ingredients except the hairpin are mixed and the fluorescent signal is measured. Then the hairpin is added to initiate the polymerization reaction and fluorescent signal is measured with 30 second intervals. After the experiment, 1 µM of product strand is added to saturate all the reporter and measure the maximum signal. The product concentration over time is then calculated as $[P] = (F(t) - F(0))/(F_{max} - F(0))$.

1.5 Gel electrophoresis experiments

To measure the PER rate without reporter complex, gel electrophoresis was used to report the product concentration. In this experiment, a total reaction volume of 60 µL was prepared in a 100 µL Eppendorf tube. FAM-labeled primer strands were used. Aliquots were taken every 5 minutes and the reaction was stopped by adding loading buffer in formamide and heat denaturing the sample at 95 ^oC for 5 minutes. The samples were then loaded into a 15 % polyacrylamide gel in a bath of 1x Tris/Borate/EDTA (TBE) buffer heated to 65 ^oC. Then 100 V was applied for 2 hours and the gels were imaged using a SynGene Genebox gel imager operated with the Genesys software. Gels were not stained so that only FAM-labeled strands were visible.

2 Supplementary Table: DNA sequences

The table below contains all DNA sequences used in this work and shows the figures in which each sequence is used. The domains are color coded such that domains of the same color are complementary. The light and dark blue sequences are primers and binding domains that vary in length to control the binding energy between the reactant and the catalyst. The red and light purple domains are template domains that control the sequence of the nascent chain. The green and purple sequences are reporter strands. Modifications are in bold: InvdT is an inverted dT modifcation on the 3' end that prevents DNA polymerase from extending the sequence, FAM is a 3' or 5' end fluorescein modification and IaBkFQ (Iowa Black FQ) is a quencher.

	Name	Sequence	Figures
1	Primer 1	TTACACTACTCTCTTATT	2,5,S2,S5,S7
2	Product 1	TTACACTACTCTCTTATTACTAAATTCA	2,5,S2,S5,S7
3	Quencher 1	**/5IaBkFQ/** TTACACTACTCTCTTATTACTA **/3InvdT/**	2,5,S2,S5,S7
4	Reporter 1	TGAATTTAGTAATAAGAGAGTAGTGTAA **/36-FAM/**	2,5,S2,S5,S7
5	HP1_length_18	ACTAAATTCAGGGCCTTTTGGCCCTGAATTTAGTAATAAGAGAGTAGTGTAA **/3InvdT/**	2,5,S2,S5,S7
6	HP1_length_16	ACTAAATTCAGGGCCTTTTGGCCCTGAATTTAGTAATAAGAGAGTAGTGT **/3InvdT/**	2,5,S2,S5,S7
7	HP1_length_14	ACTAAATTCAGGGCCTTTTGGCCCTGAATTTAGTAATAAGAGAGTAGT **/3InvdT/**	2,5,S2,S5,S7
8	HP1_length_12	ACTAAATTCAGGGCCTTTTGGCCCTGAATTTAGTAATAAGAGAGTA **/3InvdT/**	2,5,S2,S5,S7
9	HP1_length_10	ACTAAATTCAGGGCCTTTTGGCCCTGAATTTAGTAATAAGAGAG **/3InvdT/**	2,5,S2,S5,S7
10	HP1_length_8	ACTAAATTCAGGGCCTTTTGGCCCTGAATTTAGTAATAAGAG **/3InvdT/**	2,5,S2,S5,S7
11	HP1_length_6	ACTAAATTCAGGGCCTTTTGGCCCTGAATTTAGTAATAAG **/3InvdT/**	2,5,S2,S5,S7
12	Primer 2 FAM	**/56-FAM/** ATTTAATTATTATATTTATT	S6
13	Product 2 FAM	**/56-FAM/** ATTTAATTATTATATTTATT AACCTCATCC	S6
14	Primer 2	ACCATTTAATTATTATATTTATT	S6
15	Product 2	ATTTAATTATTATATTTATT AACCTCATCC	S6
16	Quencher 2	**/5IaBkFQ/** ACCATTTAATTATTATATTTATTAACC /3**InvdT/**	S6
17	Reporter 2	GGATGAGGTTAATAAATATAATAATTAAATGGT **/36-FAM/**	S6
18	HP2_length_20	AACCTCATCCGGGCCTTTTGGCCCGGATGAGGTTAATAAATATAATAATTAAAT	S6
19	HP2_length_18	AACCTCATCCGGGCCTTTTGGCCCGGATGAGGTTAATAAATATAATAATTAACC	S6
20	HP2_length_16	AACCTCATCCGGGCCTTTTGGCCCGGATGAGGTTAATAAATATAATAATTCCCC	S6
21	HP2_length_14	AACCTCATCCGGGCCTTTTGGCCCGGATGAGGTTAATAAATATAATAACCCCCC	S6
22	HP2_length_12	AACCTCATCCGGGCCTTTTGGCCCGGATGAGGTTAATAAATATAATCCCCCCCC	S6
23	HP2_length_10	AACCTCATCCGGGCCTTTTGGCCCGGATGAGGTTAATAAATATACCCCCCCCCC	S6
24	HP2_length_8	AACCTCATCCGGGCCTTTTGGCCCGGATGAGGTTAATAAATACCCCCCCCCCCC	S6
25	HP2_length_6	AACCTCATCCGGGCCTTTTGGCCCGGATGAGGTTAATAAACCCCCCCCCCCCCC	S6
26	HP2_length_4	AACCTCATCCGGGCCTTTTGGCCCGGATGAGGTTAATACCCCCCCCCCCCCCCC	S6
27	R1	**/56FAM/** TGAAGTTTGGTGGTGAGATG	4,S3,S4
28	R1'	CACCACCAAACTTCA **/3IABkFQ/**	4,S3,S4
29	R2	TGAGATGAAGTTTGGTGGTG **/36-FAM/**	4,S3,S4
30	R2'	**/5IABkFQ/** CACCACCAAACTTCA	4,S3,S4
31	R1_fullcomplement	CATCTCACCACCAAACTTCA	4,S3,S4
32	R2_fullcomplement	CACCACCAAACTTCATCTCA	4,S3,S4

3 Supplementary Discussion 1: Derivation of PER rate without helicase

Here we derive Equation (3) in the main manuscript from Equations (1) and (2). We are looking to predict the reaction rate dependence on the length of the domain that facilitates binding between the reactant and the catalyst for a given initial reactant concentration R_0 and catalyst concentration C_0.

To solve for the three unknown constant concentrations in equations 1 and 2 in the main manuscript, $[RC]$, $[PC]$, and $[C]$, we use a mass balance equation for $[C]$—the total catalyst concentration C_0 is conserved and given by $C_0 = [C] + [RC] + [PC]$—and find

$$[C] = \frac{C_0}{1 + [R]K_1\left(\frac{1+\frac{k_2}{k_{3r}}}{1+\frac{k_2}{k_{1r}}}\right) + [P]K_3}, \tag{S1}$$

where we substitute the equilibrium constants $K_1 = \frac{k_{1f}}{k_{1r}}$ and $K_3 = \frac{k_{3f}}{k_{3r}}$. Equation (S1) is a Langmuir adsorption isotherm where $[C]$ takes the role of available sorption sites, and $[P]$ and $[R]$ represent gaseous adsorbate molecules.

Because the only irreversible step in PER is the conversion of primer to product on the catalyst, the overall PER rate is $r = k_2[RC]$. Plugging this equality and into equation (S1), and assuming quasi-steady state (i.e. $[RC]$ and $[PC]$ remain constant during the reaction) so that $[RC] = [R][C]\frac{k_{1f}}{k_{1r}+k_2}$, we find

$$r = -k_2[R]\frac{K_1}{1+\frac{k_2}{k_{1r}}}\frac{C_0}{1 + [R]K_1\left(\frac{1+\frac{k_2}{k_{3r}}}{1+\frac{k_2}{k_{1r}}}\right) + [P]K_3}. \tag{S2}$$

We simplify Equation (S2) using the fact that the equilibrium constants K_1 and K_3 are approximately equal (i.e. $K_1 \approx K_3 \equiv K$), because the same domain is responsible for their binding, as shown in Figure 2. For the same reason $k_{3r} \approx k_{1r} \equiv k_r$. We furthermore use that when the catalyst concentration is low $[RC]$ and $[PC]$ are small compared to the initial reactant concentration, $[R_0]$, so that $[R]+[P] \approx R_0$. Then equation (S2) reduces to

$$r = k_2[R]C_0\frac{1}{1+\frac{k_2}{k_r}}\frac{K}{1+R_0K} \tag{S3}$$

Using the fact that $r = -\frac{d[R]}{dt}$, equation S3 becomes an ordinary linear differential equation that can simply be solved to find

$$[R] = R_0\exp(-t/\tau) \tag{S4}$$

$$[P] = R_0(1-\exp(-t/\tau)) \tag{S5}$$

where $\tau = (\frac{1}{k_2}+\frac{1}{k_r})(\frac{R_0}{C_0}+\frac{1}{KC_0})$ is the typical timescale at which the reaction proceeds. Specifically, τ indicates the time it takes for $1-1/e \approx 63\%$ of the reactant to be converted to product.

To investigate the dependence of τ on DNA length and temperature we use that k_f is independent of DNA length, sequence, or concentration under typical reaction conditions[3]. We can then rewrite τ as

$$\tau = \left(\frac{1}{k_2}+\frac{K}{k_f}\right)\left(\frac{R_0}{C_0}+\frac{1}{KC_0}\right) \tag{S6}$$

4 Supplementary Discussion 2: Connecting the model to experiments

To compare equation (3) to our experiments, we need estimates for k_f and k_2, and a relation between K (the equilibrium constant of reactant-catalyst and product-catalyst binding) and the length of the binding domain on the catalyst in number of nucleotides.

We use that the hybridization rate between reactant or product strands and catalyst strands $k_f \approx 3\times 10^6$ $\mathrm{M^{-1}s^{-1}}$ as measured by Zhang and Winfree[3].

For the relation between K and the binding domain length we use that $K = \exp[-\Delta G^o/k_BT]$. The free energy of hybridization, ΔG^o, is roughly proportional to sequence length. In our experiments, the primers are composed of only A, C and T nucleotides with no adjacent C's, so few sequence-specific effects are expected. Under these conditions thermodynamic data show that at 25^oC $\Delta G^\circ \approx 9$ kJ/mol $-(n-1)\times 5.9$ kJ/mol, and at 37^oC $\Delta G^\circ \approx 8.5$ kJ/mol $-(n-1)\times 4.8$ kJ/mol, where n is the length of the primer in nucleotides.

Plugging these numbers into equation (3) results in an expression for τ as a function of n with only k_2 as an adjustable parameter. We use k_2 as a fit parameter but have an order-of-magnitude estimate of its value based on measurements by Deng *et al.*[4]. They measured that at 25^oC a 500-nucleotide template is copied in 1400 s. Assuming that this rate is linear in domain length, that corresponds to $k_2 \approx 10^{-2}$ s^{-1} for a 10-nucleotide domain. We found that values of $k_2 = 2\times 10^{-3}s^{-1}$ at 25^oC and $k_2 = 8\times 10^{-3}s^{-1}$ at 37^oC, produce good agreement between our model and the data.

5 Supplementary Discussion 3: Derivation of PER rate with helicase

In this section we derive equation (6) in the main manuscript from equations (4) and (5). We start, as in Supplementary discussion 1, from the two rate equations that describe the changes of $[RC]$ and $[PC]$ over time

(equations (1) and (2)), but include terms to account for the unwinding of the product-catalyst complex at rate k_h (see Fig. 3a) and the unintended removal of the reactant from the catalyst with a leak rate $k_l = L \times k_h$:

$$\frac{d[RC]}{dt} = k_{1f}[R][C] - (k_{1r} + k_2 + k_l)[RC] = 0. \quad \text{(S7)}$$

$$\frac{d[PC]}{dt} = k_{3f}[P][C] - (k_{3r} + k_h)[PC] + k_2[RC] = 0. \quad \text{(S8)}$$

Here k_h is a rate constant with units s^{-1} and the leak parameter L is a dimensionless constant between 0 (perfectly selective for product-catalyst complex and no reactant-catalyst unwinding) and 1 (non-selective for product-catalyst complex, unwinds reactant-catalyst complex at equal rate). We make the same assumptions as in section 2.1 that the on rates k_{1f} and k_{3f} are approximately equal and independent of the length of the binding domain. We also assume that $k_{1r} \approx k_{3r}$ and therefore that $K_1 \approx K_3$. Combined with conservation of mass, $C_0 = [C]+[RC]+[PC]$, and under the quasi-steady-state assumption which states that $[PC]$, $[RC]$, and $[C]$ remain constant during the reaction, equations (S7) and (S8) give a steady-state unoccupied catalyst concentration

$$[C] = \frac{C_0}{1 + [R]\frac{k_f}{k_r + k_2 + Lk_h}\left(1 + \frac{k2}{k_r + k_h}\right) + [P]\frac{k_f}{k_r + k_h}}. \quad \text{(S9)}$$

Next, we use that the rate of reactant consumption is $\frac{d[R]}{dt} = -k_2[RC]$ and that $R_0 = [P] + [R]$ to find

$$\frac{d[R]}{dt} = -[R]\frac{k_2 k_f}{k_r + k_2 + k_f}\frac{C_0}{1 + (A - B)[R] + BR_0}, \quad \text{(S10)}$$

where $A = \frac{k_f}{k_r + k_2 + Lk_h}\left(1 + \frac{k2}{k_r + k_h}\right)$ and $B = \frac{k_f}{k_r + k_h}$ are constants that are lumped for brevity.

Equation (S10) only has an analytical solution for [R] as a function of t if $A - B = 0$. This is the case if $k_h = 0$ and there is no unwinding by helicase, as we have seen in Section 2.1 of the main manuscript. A and B are also equal if $L = 0$ and the helicase unwinds the reactant-catalyst complex and the product-catalyst complex with equal rates. Here, we make the rather crude approximation that $A - B = 0$ also for $L \neq 0$ and $k_h \gg 1$. This approximation ignores differences in binding strength between the reactant and product with catalyst, so that when reactant gets converted to product, the free catalyst concentration does not change. Making this simplification allows us to obtain an analytical solution for the PER rate as a function of K and k_h,

$$\frac{d[R]}{dt} = -[R]\frac{k_2 k_f}{k_r + k_2 + k_f}\frac{C_0}{1 + \frac{R_0 K}{1 + \frac{k_h}{k_r}}}, \quad \text{(S11)}$$

but the analytical approximation will overestimate the reaction rate for selective helicases with high activity (see Supplementary Fig. S1). The solution to equation (S11) is an exponential decay with typical timescale

$$\tau(k_h) = \left(\frac{1}{k_2} + \frac{K}{k_f} + L\frac{Kk_h}{k_f k_2}\right)\left(\frac{1}{KC_0} + \frac{R_0}{C_0}\frac{1}{1 + K\frac{k_h}{k_f}}\right). \quad \text{(S12)}$$

Under our approximation, the reaction rate is captured by a single time scale τ, similar to the case without helicase described in section 2.1 of the main manuscript. The only difference is that in the presence of helicase, τ is a function of k_h and L. Indeed, when considering the case of $k_h = 0$, equation (S12) reduces to the expression for τ in equation (3) in the main manuscript, in which no helicase action was considered.

We conclude by estimating the error introduced by our simplification. To that end, Supplementary Figure 1 compares the predicted change in reactant concentration $[R]$ over time calculated using the numerical solution to equation (S10) (continuous line) to that calculated using the approximate analytical solution to equation (S11) (dotted line). We find that if $L = 0$ (shown in panel a), where the difference is expected to be largest, the approximate analytical solution overestimates the rate by approximately 200 % for $k_h = 10^{-2}$ s^{-1}, by 30 % for $k_h = 10^{-3}$ s^{-1}, and by only a few percent for $k_h = 10^{-3}$ s^{-4}. Panel b shows that if the helicase is not selective, the difference between the numerical and approximate analytical solution vanishes. Fitting equation (S12) experimental data, we use $k_h = 1.3 \times 10^{-3}$ s^{-1} and $L = 0.1$, so we expect we overestimate the rate no more then 30%, a small effect compared to the rate increase of 2 orders of magnitude due to the addition of helicase that the model captured.

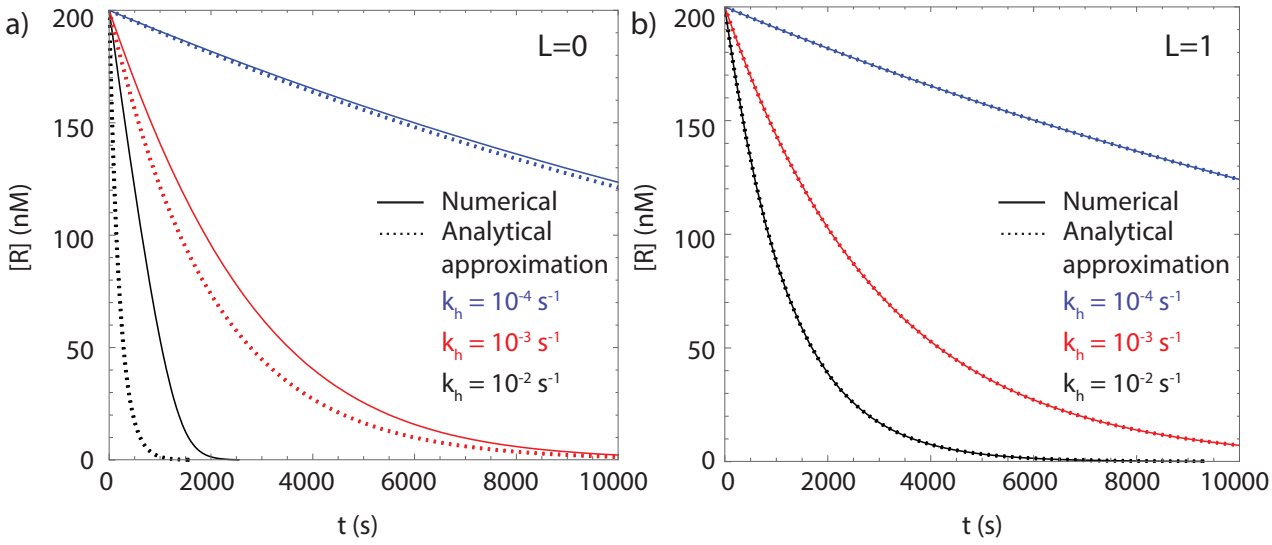

Supplementary Figure 1: Comparison between the numerical solution to equation (S10) (continuous lines) and the analytical solution to equation (S11) (dotted lines). The comparison is made at three different helicase rate constants: $k_h = 10^{-4}$ s^{-1} (black), $k_h = 10^{-3}$ s^{-1} (red), and $k_h = 10^{-2}$ s^{-1} (blue). For reference, in the comparison to experiments we use $k_h = 1.3 \times 10^{-3}$ s^{-1}. The case of a selective helicase with $L = 0$ is depicted in panel (a) and the case of a non-selective helicase with $L = 1$ is depicted in panel (b). The other parameters used are: $C_0 = 100$ nM, $R_0 = 200$ nM, $T = 298$ K, $k_f = 3 \times 10^{-6}$ M^{-1} s^{-1}, $k_2 = 2 \times 10^{-3}$ s^{-1}, and the binding domain length is 18 nucleotides.

6 Supplementary figures

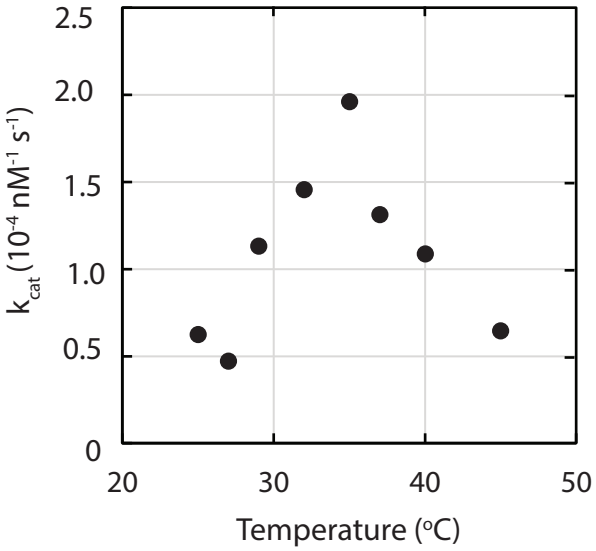

Supplementary Figure 2: Catalytic reaction rate as a function of temperature. The binding domain on the catalytic hairpin is a 10 nucleotide AGT sequence (HP_length_10 in Supplementary Table 1.)

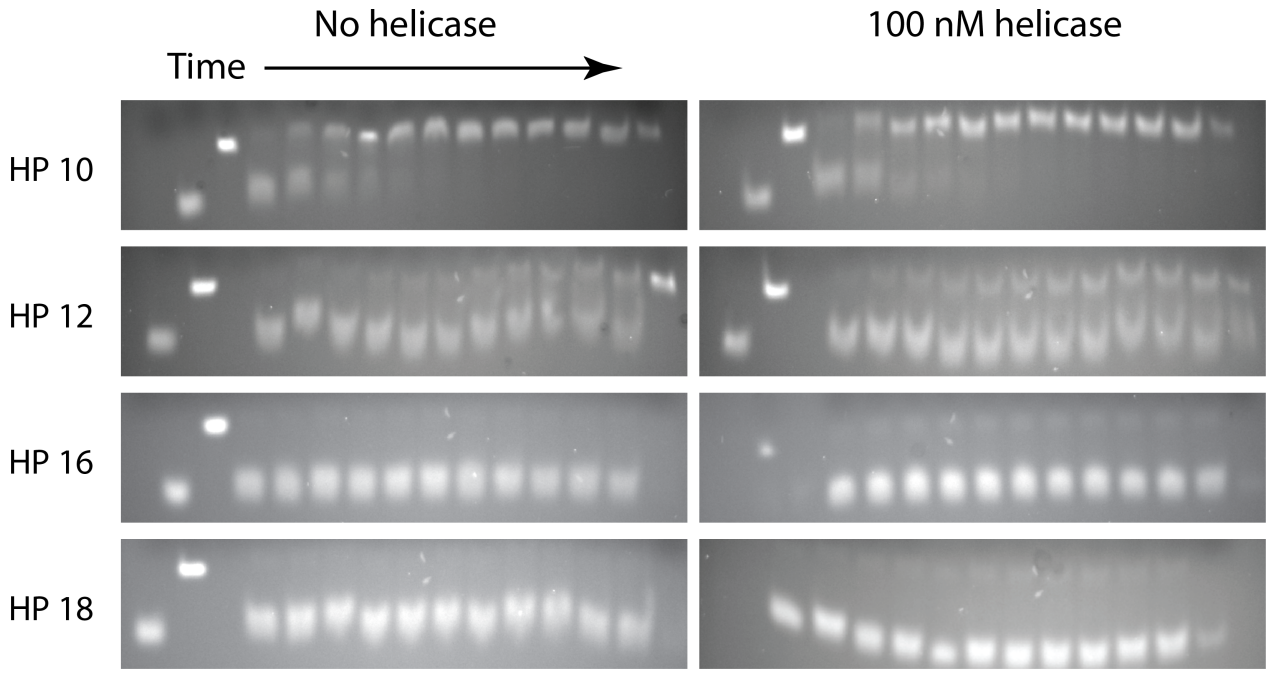

Supplementary Figure 3: Gel electrophoresis measurements of the PER rate as a function of time. The first two wells contain reactant and product strand respectively, except in the gels with 16 and 18 nucleotide long binding domains and 100 nM helicase. Each well is separated by 5 minutes and the first well is immediately after addition of RepX (0 minutes).

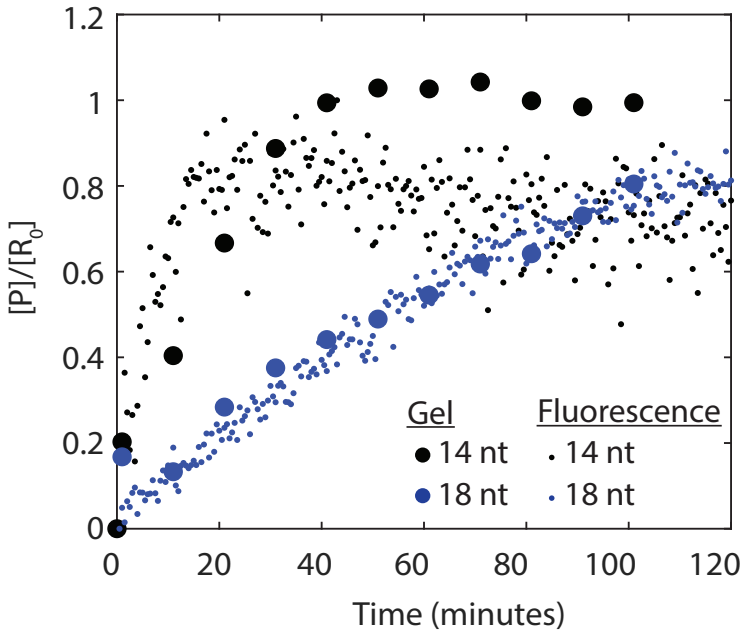

Supplementary Figure 4: We measure the PER rate using a reporter complex that reacts with the PER product and results in a fluorescent signal. To ensure that the reaction between product and reporter is not rate limiting, we measured the PER rate also using gel electrophoresis where no reporter is required. The graph shows the fraction of converted reactant over time measured both in gel electrophoresis and fluorescence experiments. The rate measurements agree fairly well. Experimental conditions are 100 nM of reactant and reporter and 10 nM of catalyst strand.

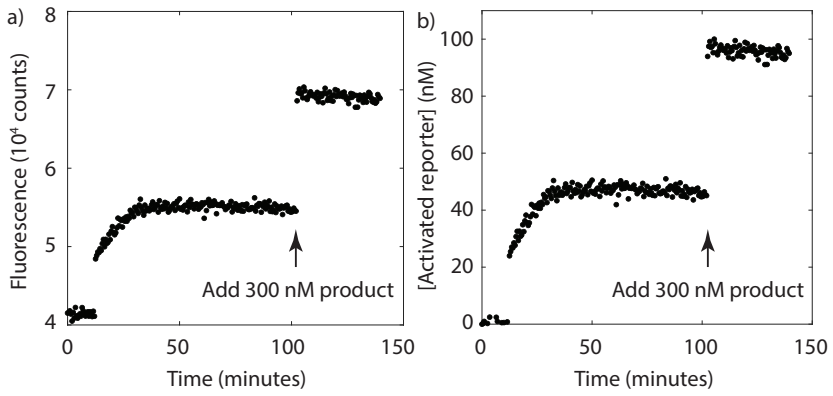

Supplementary Figure 5: Conversion of fluorescence signal to product concentration. a) Raw data of fluorescence obtained in an experiment where 100 nM reactant gets converted to product via PER with 10 nM hairpin with a 10-nucleotide binding domain, in the presence of 100 nM reporter complex and 100 nM RepX helicase. After the product is formed, it quickly reacts with the reporter complex to produce a fluorescent signal (Fig. 2b). After 100 minutes, 300 nM of product strand is added to saturate the 100 nM of reporter and obtain the fluorescent signal that corresponds to a completed reaction. b) The concentration of activated reporter as a function of time is calculated from the raw data in panel (a) as $[Activated\ reporter](t) = F(t) - F(0)/(F_{max} - F(0)0$, where $F(t)$ is the raw fluorescence counts over time. Since the reaction between reporter and product ($k_{rep} \approx 10^{-3}$ nM^{-1}s^{-1}) is much faster than the production of product ($k_{cat} < 10^{-4}$ nM^{-1}s^{-1}), the active reporter concentration over time is a reasonable estimate of the product concentration over time.

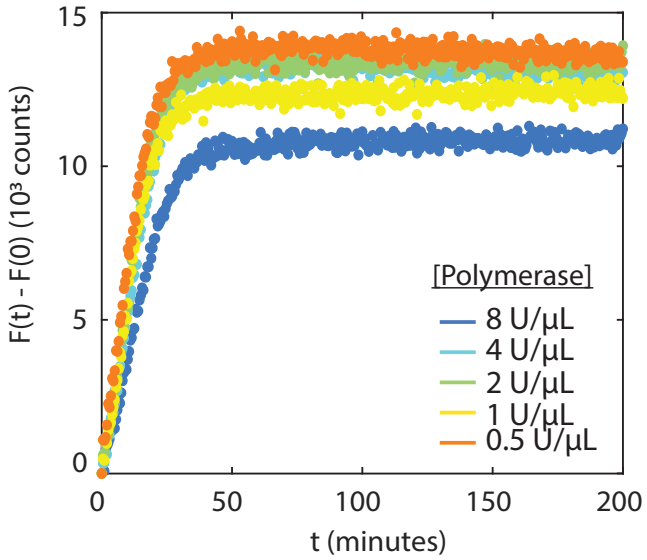

Supplementary Figure 6: Polymerization is not the rate-limiting step in PER. The graph shows fluorescence increase, which signals increased PER product, as a function of time. All PER rate measurements use a polymerase concentration of 8 U/µL. Here, we decreased the polymerase concentration down to 16-fold and find that decreasing the polymerase concentration does not systematically decrease the reaction rate, indicating that polymerization is not the rate limiting step. Instead, higher DNA polymerase concentrations appear to slightly decrease the initial rate which could be related to the viscosity of the fluid, as the DNA polymerase is stored in a 50% glycerol mixture. The reaction mixture contained 200 nM reactant and reporter and 10 nM hairpin with a 14-nucleotide binding domain. The reaction was performed at 37 ^oC.

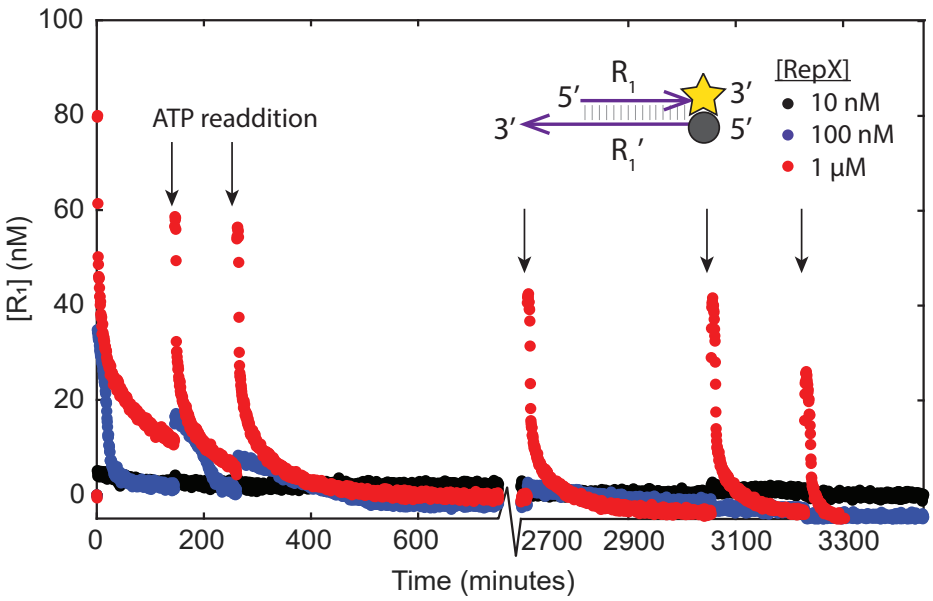

Supplementary Figure 7: RepX activity decrease over time is due to ATP depletion. The y axis shows the concentration of unhybridized R_1 strand, which is a measure for helicase activity. Black arrows indicate time times when of ATP is added to a final concentration of 1 mM. The renewed activity in response to ATP addition shows that the activity decrease over time is due to ATP depletion. Sample contains 100 nM RepX and 100 nM of $R_1 : R_1'$ complex.

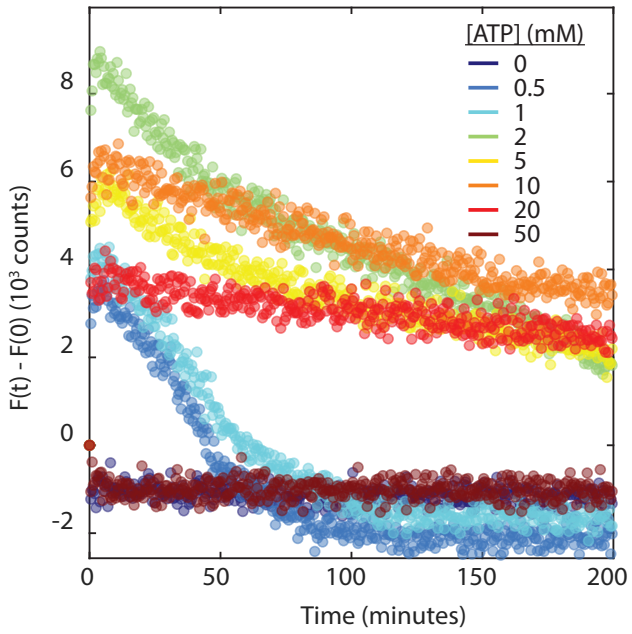

Supplementary Figure 8: RepX activity at various ATP concentrations. The y-axis shows fluorescent signal in counts which signals helicase activity. Helicase unwinds a reporter complex, separating a fluorophore from a quencher, thereby increasing the signal. Each sample contains 100 nM of RepX helicase, 100 nM of reporter complex and varying amounts of ATP. More ATP tends to enable RepX to retain its activity for longer times. No activity is observed at 0 mM ATP and 50 mM ATP.These results suggest that high concentrations of ATP inhibit RepX activity.

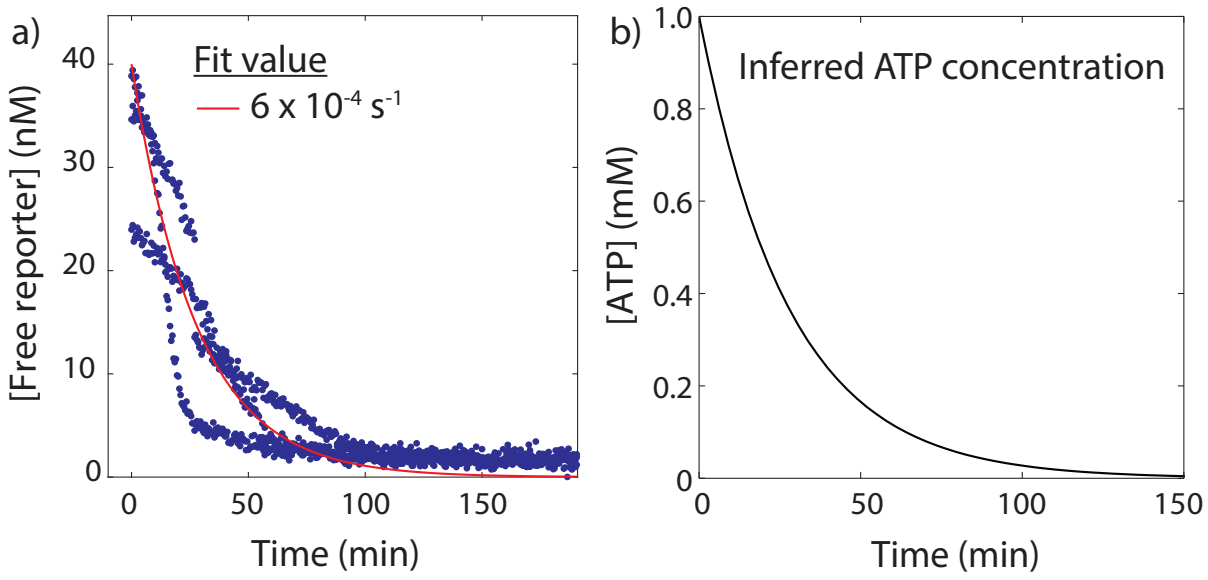

Supplementary Figure 9: Estimate of the ATPase rate of RepX under conditions relevant to the primer exchange reaction. a) Concentration of unhybridized reporter due to strand-separating action of RepX. The blue dots represent three independent measurements using 100 nM DNA reporter, 100 nM RepX, and 1 mM ATP. (Same data as in Figure 4b of main manuscript). The red line is an exponential fit with k_{ATP}, the ATPase rate, and the maximum free reporter concentrations as the only fit parameters. We find that $k_{ATP} \approx 6 \times 10^{-4}$ s^{-1}. That means that 1 RepX molecule converts approximately 6 ATP molecules per second under the given conditions. b) Inferred ATP concentration over time using the fit value from panel (a).

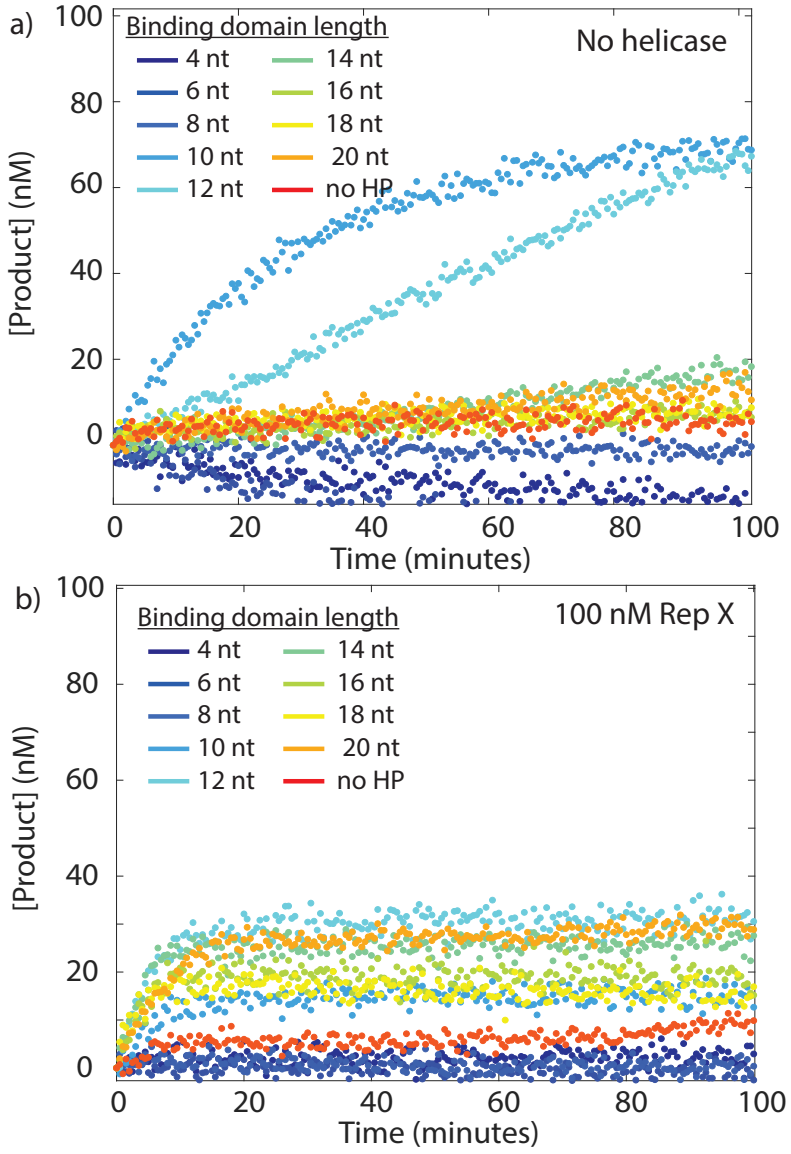

Supplementary Figure 10: PER product over time in the presence (a) and absence (b) of 100 nM of RepX helicase and 1 mM ATP. The sample also contains 200 nM primer and 10 nM of catalytic hairpin with variable binding domain length. Reactions were performed at 25 ^oC. The addition of helicase increases the PER rate for binding domains longer than the optimal domain length of 8 nucleotides, but decreases the yield. The yield decrease is likely due to RepX unwinding and deactivating the catalytic hairpins. To address the issue of reduced yield, we increased the hairpin concentration from 10 nM to 100 nM (Fig. 5).

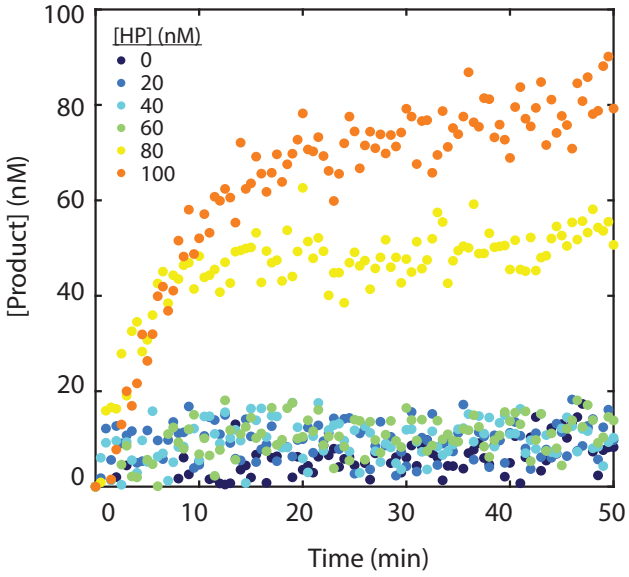

Supplementary Figure 11: Yield of PER in the presence of RepX helicase increases with increasing hairpin concentration. The product concentration over time for a PER reaction containing 100 nM RepX helicase, 1 mM ATP, 200 nM primer and reporter and varying amounts of hairpin with a 12-nucleotide binding domain is shown.

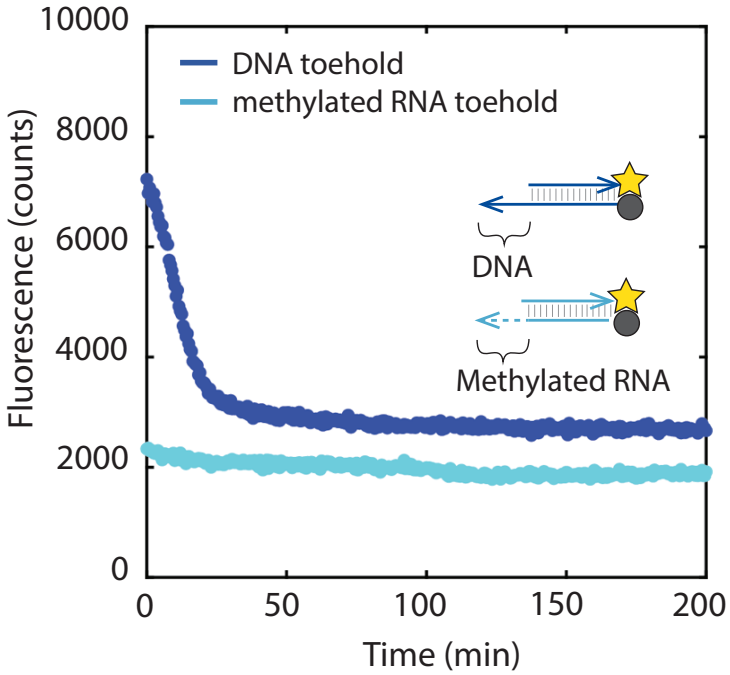

Supplementary Figure 12: RepX does not recognize DNA complexes with a 3' methylated RNA toehold as substrates. The fluorescent signal is a measure for the fraction of opened reporter strand. The dark blue complex represents a DNA reporter. The light blue complex represents a DNA reporter where all 5 DNA nucleotides in the 3' toehold are replaced by their methylated RNA 3' equivalent.

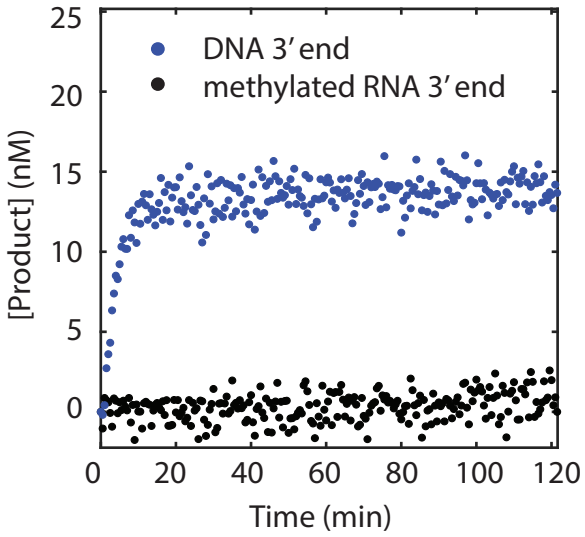

Supplementary Figure 13: Converting the 3' toehold of PER hairpins to methylated RNA is not a good way to protect those hairpins from unwinding by RepX during a PER reaction, because Bst Polymerase also does not recognize the hairpins with methylated RNA toeholds as templates. The product concentrations over time are shown for PER reactions containing 100 nM RepX helicase, 1 mM ATP, 200 nM primer and reporter and 100 nM catalytic hairpin with a 16-nucleotide binding domain composed either entirely of DNA or composed of DNA except for the 3' toehold, which is methylated RNA. The reaction proceeds quickly when the hairpin is entirely made of DNA (blue dots). The reaction does not proceed at all when the first 13 bases on the 3' end are replaced by their methylated RNA counterparts.

7 Notes on references

To facilitate finding relevant information, we added a sentence to each reference either pointing the reader to the specific graph, table, or value that that was used in this work or briefly summarizing the point of the paper and why it was cited.

[1] Neville R. Kallenbach, Rong-Ine Ma, Nadrian C. Seeman, *Nature* 1983, **305**, 829-831. Experimental introduction of designed stable DNA junctions that underlie much of structural DNA nanotechnology.

[2] Bernard Yurke, Andrew J. Turberfield, Allen P. Mills Jr., Friedrich C. Simmel & Jennifer L. Neumann, *Nature* 2000, **406**, 605-608. Introduction of designed DNA strand-displacement reactions that underlie many dynamical DNA nanotechnology.

[3] Yaakov Benenson, Binjamin Gil, Uri Ben-Dor, Rivka Ador & Ehud Shapiro, *Nature* 2004, **429**, 423-429. Demonstrates the power of DNA nanotechnology by building a DNA computer that recognizes disease-related mRNA in vitro and produces an output DNA.

[4] Randolph Lopez, Ruofan Wang & Georg Seelig, *Nature Chemistry* 2018, **10**, 746-754. Experimentally built a DNA computer that recognizes patterns in mRNA concentration that signal disease.

[5] Paul W. K. Rothemund, *Nature* 2006, **440**, 297-302. Demonstration of DNA origami: the folding of DNA into complex well-defined 2D shapes.

[6] Swarup Dey, Chunhai Fan, Kurt V. Gothelf, Jiang Li, Chenxiang Lin, Longfei Liu, Na Liu, Minke A. D. Nijenhuis, Barbara Saccà, Friedrich C. Simmel, Hao Yan & Pengfei Zhan, *Nature Reviews Methods Primers* 2021, **1**, 13. Reviews methods, applications, and understanding of DNA origami.

[7] Guido Grossi, Mette Dalgaard Ebbesen Jepsen, Jørgen Kjems & Ebbe Sloth Andersen, *Nature Communications* 2017, **8**, 992. Built a reconfigurable DNA box that contains an enzyme to control its activity.

[8] Ebbe S. Andersen, Mingdong Dong, Morten M. Nielsen, Kasper Jahn, Ramesh Subramani, Wael Mamdouh, Monika M. Golas, Bjoern Sander, Holger Stark, Cristiano L. P. Oliveira, Jan Skov Pedersen, Victoria Birkedal, Flemming Besenbacher, Kurt V. Gothelf & Jørgen Kjems, *Nature* 2009, **459**, 73-76. Demonstrated a reconfigurable DNA origami in the form of a box with a lid that opens on demand.

[9] Anton Kuzyk, Maximilian J. Urban, Andrea Idili, Francesco Ricci & Na Liu. *Science Advances* 2017, **4**, e160280. Demonstrate a pH-sensitive DNA-based plasmonic structure.

[10] Heini Ijäs, Iiris Hakaste, Boxuan Shen, Mauri A. Kostiainen & Veikko Linko. *ACSNano* 2019, **13**, 5959–5967. Updated origami box that opens in response to pH changes.

[11] Leonard M. Adleman, *Science* 1994, **266** 1021-1024. Experimental demonstration of a DNA-based computation.

[12] Georg Seelig, David Soloveichik, David Yu Zhang & Erik Winfree, *Science* 2006, **314** 1585-1588. Experimental demonstration of DNA logic gates.

[13] Kevin M. Cherry & Lulu Qian, *Nature* 2018, **559**, 370-376. Demonstration of a DNA-based neural network that performs pattern recognition tasks.

[14] John SantaLucia Jr, *Biochemistry* 1996, **35**, 3555–3562. Values based on table 3.

[15] John SantaLucia Jr, *Proc. Natl. Acac. Sci. USA* 1998, **95**, 1460-1465. The sequence-dependence of hybridiziation energy is explained using the Nearest-Neighbor Model.

[16] David Yu Zhang, Sherry Xi Chen & Peng Yin, *Nature Chemistry* 2012, **4**, 208-214. Lowest theoretical upper bound value taken from the mismatch case in Figure 1c.

[17] David Yu Zhang & Georg Seelig, *Nature Chemistry* 2011, **3**, 103-113. Review showing various DNA-strand displacement circuits. Most occur over many hours.

[18] Kevin M. Cherry & Lulu Qian, *Nature* 2018, **559**, 370-376. Developed a neural network that operates on the timescale of 3 to 20 hours based on DNA hybridization reactions involving over 100 strands.

[19] Kevin Montagne, Raphael Plasson, Yasuyuki Sakai, Teruo Fujii & Yannick Rondelez, *Mol. Sys. Bio.* 2011, **7**, 466. First introduction of the PEN toolbox.

[20] Jocelyn Y. Kishi, Thomas E. Schaus, Nikhil Gopalkrishnan, Feng Xuan & Peng Yin, *Nature Chemistry* 2018, **10**, 155-164. First introduction of the primer exchange reaction. Fig. 2d shows the optimal rate.

[21] Lulu Qian & Erik Winfree, *Science* 2011, **332**, 1196-1201. Showed computations that include seesaw-gates which rely on the reversible binding of 5-nucleotide toeholds and operate on the timescale of hours.

[22] Gadi Rothenberg. Catalysis: Concepts and Green Applications. John Wiley &Sons, Ltd. Publising, 2008. Textbook on the basics of catalysis. Sabatier's principle is discussed in section 2.3.

[23] J. N. Milligan & A. D. Ellington, *Chemical Communications* 2015, **51**, 9503-9506. Used RecA to modulate binding energy in catalytic DNA reactions and thereby speed them up.

[24] Guillaume Gines, Roberta Menezes, Kaori Nara, Anne-Sophie Kirstetter, Valerie Taly & Yannick Rondelez, *Science Advances* 2020, **6**, 6. Used PEN-toolbox for sensitive micro RNA detection.

[25] Sinem K. Saka, Yu Wang, Jocelyn Y. Kishi, Allen Zhu, Yitian Zeng, Wenxin Xie, Koray Kirli, Clarence Yapp, Marcelo Cicconet, Brian J. Beliveau, Sylvain W. Lapan, Siyuan Yin, Millicent Lin, Edward S. Boyden, Pascal S. Kaeser, German Pihan, George M. Church & Peng Yin, *Nature Biotechnology* 2019, **37**, 1080-1090. Used PER to amplify signal in an in-vivo protein imaging tool.

[26] G. Gines, A. S. Zadorin, J.-C. Galas, T. Fujii, A. Estevez-Torres & Y. Rondelez, *Nature Nanotechnology* 2017, **12**, 351-359. Built reaction networks using PEN toolbox that controls positioning of microscopic particles.

[27] Anton S. Zadorin, Yannick Rondelez, Guillaume Gines, Vadim Dilhas, Georg Urtel, Adrian Zambrano, Jean-Christophe Galas & Andé Estevez-Torres, *Nature Chemistry* 2017, **2017**, 990-996. Used PEN toolbox to create spatial pattern that controlled particle aggregation.

[28] Thomas E. Schaus, Sungwook Woo, Feng Xuan, Xi Chen & Peng Yin, *Nature Communications* 2017, **8**, 696. Used PER to built a molecular-event recorder that tracks the sequence in which molecules have been in close proximity.

[29] Sinan Arslan, Rustem Khafizov, Christopher D. Thomas, Yann R. Chemla & Taekjip Ha, *Science* 2015, **348**, 344-347. Engineering and characterization of Rep-X helicase.

[30] David Yu Zhang, Erik Winfree, *J. Am. Chem. Soc.* 2009, **131**, 17303-17314. Introduction of theoretical model to predict toehold-mediated DNA strand-displacement rates and its experimental validation. $k_f = 3{\times}10^6$ M/s from Fig. 3 was used.

[31] Kenneth A. Johnson & Roger S. Goody, *Biochemistry* 2011, **50** 8264-8269. Translation of 1913 paper by Michaelis and Menten on enzyme kinetics. Our derivation is based on this paper.

[32] Yingnan Deng, Liang Ma, Qianqian Han, Changyuan Yu, Alexander Johnson-Buck & Xin Su, *Nano Lett.* 2020, **20**, 2688-2694. Measurements of polymerization rate at different temperatures are estimated based on Figure S7.

[33] Jamal Temsamani, Michael Kubert & Sudhir Agrawal, *Nucleic Acid Research* 1995, **23**, 1841-1844. Sequence analysis of incomplete side products formed during DNA synthesis shows that deletions occur anywhere in the strand with increased frequency near the 3' end.

[34] Tsugunori Notomi, Hiroto Okayama, Harumi Masubuchi, Toshihiro Yonekawa, Keiko Watanabe, Nobuyuki Amino & Tetsu Hase, *Nucleic Acids Research* 2000, **28**, 63. First introduction of LAMP, an isothermal DNA amplification tool that uses Bst polymerase to displace strands.

[35] David Yu Zhang, Andrew J. Turberfield, Bernard Yurke & Erik Winfree, *Science* 2007, **16** 1121-112. First experimental work to show an isothermal autocatalytic DNA reaction.

[36] Henry Hess, 2018, arXiv preprint arXiv:1803.07415. Theoretical work asking the minimum rate of energy dissipation required for a molecular machine to speed up a chemical reaction.

[37] J. J. Hopfield, *Proc. Natl. Acad. Sci.* **71**, 1974, 4135-4139. Theoretical work showing that a dissipative process can decrease error rates in templated reactions.

References

[1] Jocelyn Y. Kishi, Thomas E. Schaus, Nikhil Gopalkrishnan, Feng Xuan & Peng Yin, *Nature Chemistry* 2018, **10**, 155-164. The relevant procedure is in methods section.

[2] Sinan Arslan, Rustem Khafizov, Christopher D. Thomas, Yann R. Chemla & Taekjip Ha, *Science* 2015, **348**, 344-347. The relevant procedure is in methods section.

[3] David Yu Zhang, Erik Winfree, *J. Am. Chem. Soc.* 2009, **131**, 17303-17314. Introduction of theoretical model to predict toehold-mediated DNA strand-displacement rates and its experimental validation. $k_f = 3 \times 10^6$ $\mathrm{M}^{-1}\mathrm{s}^{-1}$ from Fig. 3 was used.

[4] Yingnan Deng, Liang Ma, Qianqian Han, Changyuan Yu, Alexander Johnson-Buck & Xin Su, *Nano Lett.* 2020, **20**, 2688-2694. Measurements of polymerization rate at various temperatures are estimated based on Figure S7.